# Pore Perfection vs. Defect Design: Examining the Complex Relationship Between Pore Structure and Carbon Dioxide Adsorption in Zr-Based MOFs.

Mason C. Lawrence,[a] Aidan M. Spoel, [a] Michael J. Katz [a,*]

Department of Chemistry, Memorial University of Newfoundland, St. John's, Newfoundland and Labrador, Canada A1B 3X7

*KEYWORDS: Metal-Organic Frameworks, carbon dioxide sequestration, enthalpy of adsorption, UiO. UiO-66, UiO-67*

**ABSTRACT:** This work examines the relationship between defects, pore size, and pore functionalization as it pertains to the enthalpy of adsorption between carbon dioxide and zirconium-based metal-organic frameworks (UiO-66 and UiO-67). When UiO-66 is synthesized without defects, carbon dioxide adsorption is more exothermic relative to when UiO-66 contains defects (–24.3 vs. –20.9 kJ/mol). We repeated the experiments with pristine/defective UiO-67 and observed the opposite trend (–16.9 vs. –21 kJ/mol), albeit less exothermic. Dehydrating the cluster of pristine/defective UiO-66 (–21 kJ/mol) and UiO-67 (–14 kJ/mol) the adsorption capabilities decreased considerably. This work indicates that there is a hierarchy of adsorption interactions that can work independently or in tandem to increase the enthalpy of adsorption. These include the small tetrahedral pore of UiO-66, hydrogen bonding, and dispersion interaction enhanced by the electron-withdrawing Zr(IV). Post-synthetic modification of the node with methanol/methoxy groups had a strong effect on the defect containing UiO-66. In this MOF, the pore sizes appeared nearly identical to the pristine UiO-66 and contained an enthalpy adsorption of –28 kJ/mol; this is the highest value obtained in this work.

## 1 Introduction

Given the role of carbon dioxide on climate change,[1-4] it is no surprise that companies, industries, and countries have set a target to reduce the net carbon dioxide emissions to zero by 2050 (net-zero).[5-8] This challenge is multi-faceted but can be over-simplified to three approaches. One approach is to develop new infrastructure that doesn't rely on carbon dioxide producing systems.[9] The second approach is to capture carbon dioxide emissions at the source;[10-15] for combustion, this is approximately 15% of the exhaust stream.[13] The last is to capture carbon dioxide in the atmosphere at ca. 400 ppm.[15-19] While the first approach may be the most obvious, it may require considerable time for infrastructure development;[6, 8-9] this assumes a solution is possible. For the latter two methods, carbon dioxide capture from emission sources is easier due to the notably higher carbon dioxide partial pressure,[12] but the challenge associated with competitive binding (e.g., water) must be addressed.[20-22] With that in mind, materials capable of adsorbing carbon dioxide over other gases will play a critical role for the net-zero target.[23-24]

Metal-organic frameworks (MOFs) – with their tunable pore apertures, pore size, and pore functionality – are already being implemented in carbon dioxide sequestration.[18, 21, 25-26] Further development of MOFs will further benefit their implementation.[13, 22, 27-31] For optimal adsorption, the ideal material would bind carbon dioxide with a high exothermic enthalpy of adsorption. This would ensure that carbon dioxide is not released prematurely. The contraposition is that the energetic, and thus financial, penalty for regeneration of the MOF (i.e., the endothermic enthalpy of desorption) must be minimized; barring hysteresis in the isotherm or forms of triggered structural changes, the enthalpy of adsorption and desorption are the same.[32-33] Thus, there exists an optimal enthalpy of adsorption for selective carbon dioxide sequestration. The upper limit of physisorption is -60 kJ/mol, beyond this point temperature/pressure swing adsorption and release is no longer possible.[34-37]

Given the multitude of node/linker combinations available for MOF design/synthesis,[38-39] there are many structure-property relationships that have explored carbon dioxide adsorption.[40-45] While most structure-property relationships focus on the role of steric and/or electronic effects via pendent groups on the node/linkers, we are interested in examining the role of defects on carbon dioxide adsorption. Defects are inherent to all materials. Thus, each synthetic protocol of a material has a specific defect density. Controlling defects in the UiO family of MOFs has been well established.[46-49] In UiOs, zirconium-cluster based nodes ($Zr_6O_4(OH)_4^{+12}$) are connected via linear ditopic dicarboxylate linkers (L) to form a topology consisting of a large octahedral pore that face share with eight smaller tetrahedral pore.

The present work sets out to determine what structural features of the UiO family are necessary for the efficient adsorption of carbon dioxide. The work examines UiO-66 (L = terephthalate; BDC) and UiO-67 (L = biphenyldicarboxylate; BPDC). Using acetic acid or hydrochloric acid as the

modulators, pristine and defective (respectively) UiOs can be synthesized.[46, 50-54] The defects are either missing linker, missing node, or a combination of both.[49-50] In the present work, missing linkers are believed to be the dominant defect. The missing linkers are either replaced by capping carboxylate groups or terminal water/hydroxide groups on the node. Given this, defect-rich UiO-66 would contain larger pores, more hydrogen bonding sites, and potentially metal sites that a guest can bind with. Furthermore, post synthetically, the node of the MOF can be dehydrated ($Zr_6O_6^{12+}$)[55] or the terminal groups can be replaced with methanol/methoxy groups.[56] Based on these six variants of UiO-66 and UiO-67, we demonstrate the importance of the pore size, specifically the tetrahedral pore, coupled with hydrogen bonding and dispersion effects in UiO-66 on carbon dioxide adsorption.

## 2 Methods

The Supporting Information (SI) file contains details for the synthesis and powder X-ray diffractograms (Figure S1 &S2) of all materials examined herein.

Nitrogen gas adsorption isotherms were measured on a Micromeritics 3Flex instrument. The samples were maintained at 77 K over the course of the run. Prior to gas adsorption measurements samples were prepared (activated) on a Micrometrics Smart VacPrep instrument. Apart from the thermally dehydrated samples that had to be heated to 573 K, all samples were activated by first heating the samples to 363 K at a rate of 5 °/min while the pressure was simultaneously reduced at 5 mmHg/s. The temperature was maintained for 30 min. Subsequently, samples were heated to 423 K at a rate of 5 °/min and held for 600 min.

Dehydrated node UiOs (ΔUiO-66-AA, ΔUiO-66-HCl, ΔUiO-67-AA, and ΔUiO-67-HCl) were synthesized/activated from the parent material on a Micrometrics Smart VacPrep instrument. The samples were initially evacuated at 5 mmHg/s while the sample was heated to 363 K at a rate of 5 °/min. Once the pressure and temperature were stable, the sample was maintained at this temperature and reduced pressure for 30 min. Subsequently, the samples were heated to 423 K at 5 °/min and held for 60 min. In the final heating step, the samples were heated to 573 K at a heating rate of 5 °/min and held for 540 min.

Carbon Dioxide isotherms were measured on a Micrometrics 3Flex instrument. The samples were maintained at a constant temperature with the use of a VWR water recirculating bath. The temperature the isotherms were measured at 278 K, 283 K, and 288 K.

$$Q_{ads} = Q_{max}\frac{K_{ads}P}{(1+K_{ads}P)} + c \quad (1)$$

$$lnK_{ads} = -\frac{\Delta H}{RT} + \frac{\Delta S}{R} \quad (2)$$

Thermodynamic parameters and maximum adsorption capacity for each MOF were extracted by first fitting the isotherms to the single site Langmuir equation (Equation 1; $K_{ads}$ is the equilibrium constant, $P$ is pressure, $Q_{max}$ is the maximum adsorption capacity, and $Q_{ads}$ is the quantity adsorbed at $P$). In the fitting process, each sample was fit to a global $Q_{max}$. Additionally, an offset parameter ($c$) was used to account for any adsorption/leak from the sample holder. Subsequently, the Van 't Hoff equation (Equation 2) was used to extract the enthalpy and entropy of adsorption from the slope and intercept, respectively. Table S1 & S2 in the SI contains the fit parameters from this work.

## 3 Results and Discussion

**Table 1: Nitrogen gas accessible Brunauer, Emmett, Teller (BET) surface area, and carbon dioxide adsorption capacity and enthalpy of adsorption for the UiOs in this work.**

| | BET Surface Area[a] ($m^2/g$) | $Q_{max}$[b,c] (mmol/g) | $\Delta H_{ads}$[b,c] (kJ/mol) |
|---|---|---|---|
| UiO-66-AA | 1725 | 6.84 ± 0.03 | −24.3 ± 1.5 |
| UiO-66-HCl | 1600 | 7.15 ± 0.03 | −20.9 ± 0.7 |
| UiO-67-AA | 1520 | 5.87 ± 0.06 | −17 ± 4 |
| UiO-67-HCl | 2400 | 8.93 ± 0.12 | −21 ± 3 |
| ΔUiO-66-AA | 1480 | 8.01 ± 0.06 | −21.4 ± 1.4 |
| ΔUiO-66-HCl | 1550 | 8.02 ± 0.04 | −21.1 ± 1.0 |
| ΔUiO-67-AA | 1540 | 9.53 ± 1.5 | −13 ± 4 |
| ΔUiO-67-HCl | 2130 | 10.64 ± 0.18 | −14 ± 4 |
| MeOH-UiO-66-AA | 1450 | 5.22 ± 0.03 | −23.5 ± 1.7 |
| MeOH-UiO-66-HCl | 1420 | 7.91 ± 0.05 | −28 ± 2 |
| MeOH-UiO-67-AA | 2440 | 7.70 ± 0.09 | −19.4 ± 1.7 |
| MeOH-UiO-67-HCl | 2100 | 7.18 ± 0.07 | −20 ± 3 |

[a] determined from nitrogen gas adsorption isotherms
[b] determined from carbon dioxide gas adsorption isotherms
[c] Tables S1 and S2 contain the Langmuir and Van 't Hoff fit parameters (including $\Delta S_{ads}$), and information regarding errors.

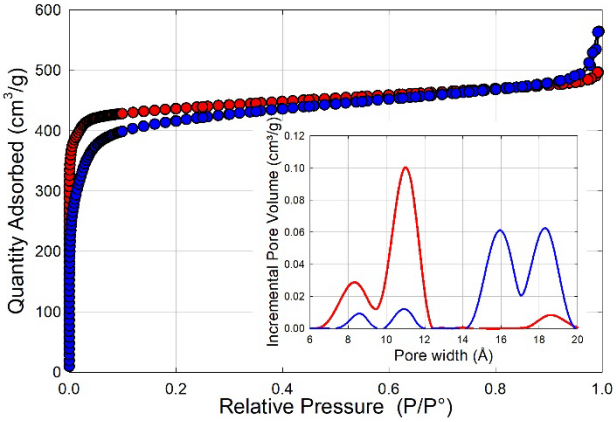


Figure 1: UiO-66-AA (red) and UiO-66-HCl (blue). Nitrogen gas accessible adsorption isotherms measured at 77 K. Inset illustrates the associated PSDs using the cylindrical pores on an oxide surface (standard deviation of fit: 7.05 and 1.59 $cm^3/g$, respectively).

UiO-66-AA and UiO-66-HCl, were formed via the reaction of Zr(IV) chloride and terephthalic acid ($H_2BDC$) in *N,N*-dimethylformamide (DMF) using either acetic acid[57] as the modulator, or hydrochloric acid as the modulator.[50] The synthesis of UiO-66-AA is known to produce pristine UiO-66 that contain little to no missing linkers.[20, 51] For UiO-66-HCl, it

has been estimated that 1-2 of the 6 linkers are missing.[20, 50, 58] For every missing linker, the zirconium defect sites are capped with two water molecules and two hydroxide molecules; this retains the coordination chemistry and charge neutrality of the MOF.[20, 59] In addition to missing linkers, missing nodes are also possible.[49] This is likely a necessity as the number of missing linkers increases. The effect of defects can be seen in the pore size distribution (PSD) shown in Figure 1. For UiO-66-AA, there are no pores larger than ca. 12 Å, consistent with the octahedral pore (12 Å).[48, 58] For UiO-66-HCl the dominant pores are all larger than the expected pore sizes, which illustrates the presence of defects that lead to larger-than-expected pore sizes.

The carbon dioxide adsorption isotherms for UiO-66-AA and UiO-66-HCl (Figure 2) were measured at 278, 283, and 288 K and clearly demonstrate the superior behavior of UiO-66-AA. To better ascertain the origin of these differences, the isotherms were fit to a single-site Langmuir isotherm (Equation 1).[34] From the equilibrium constants obtained (Table S1), the enthalpy of gas adsorption was extracted using the van 't Hoff relationship (Table S2).

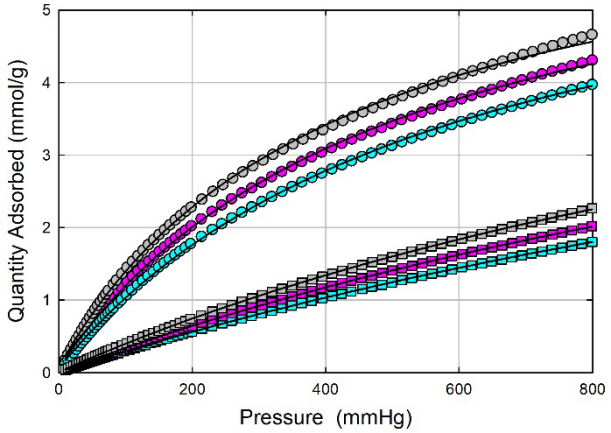


Figure 2: Carbon dioxide adsorption isotherms of UiO-66-AA (circles) and UiO-66-HCl (squares) at 278 K (grey) 283 K (pink) and 288 K (cyan). The fits from the Langmuir isotherm model are shown as black lines.

As shown in Table 1, the maximum adsorption capacity ($Q_{max}$) between UiO-66-AA and UiO-66-HCl is similar (6.84 vs. 7.15 mmol/g respectively); on a per mole basis, these values are identical (11.2 and 11.3 mol $CO_2$/mol MOF). The key difference is in the enthalpy of adsorption. Carbon dioxide adsorption on UiO-66-AA is 3.4 kJ/mol more exothermic than in UiO-66-HCl (–24.4 kJ/mol vs. –20.9 kJ/mol). For UiO-66-AA, the enthalpy of adsorption is close to the computationally calculated value of –26.2 kJ/mol by Maurin and co-workers and close to the experimentally determined value of –26 kJ/mol by Walton and coworkers.[17,18]

We propose two hypotheses to explain this behaviour: The pristine material contains surface binding sites (e.g., edges/corners) that are favourable for carbon dioxide adsorption. Alternatively, it is possible that one of the two pore sizes (tetrahedral or octahedral) is a better fit to tightly bind carbon dioxide. To explore these hypotheses, we repeated the adsorption experiments with UiO-67-AA and UiO-67-HCl, which contain larger pores due to the longer biphenyl dicarboxylate linker. If we observe similar behaviour for UiO-67 as with UiO-66, then the former hypothesis is consistent with the data; if a different behaviour is observed, then the latter hypothesis is consistent with the data.

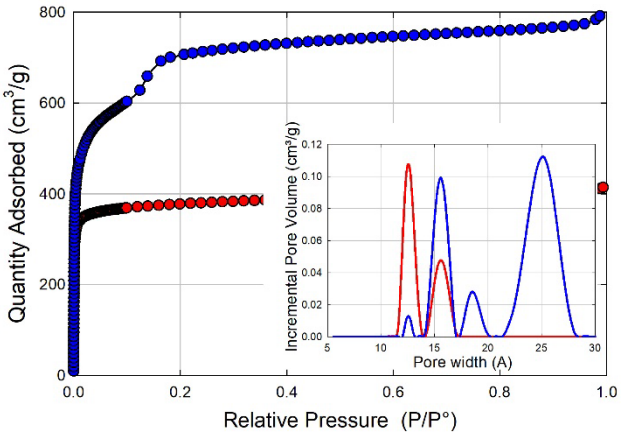


Figure 3: UiO-67-AA (red) and UiO-67-HCl (blue). Nitrogen gas accessible adsorption isotherms measured at 77 K. Inset illustrates the associated PSDs using the cylindrical pores on an oxide surface (standard deviation of fit: 23.25 and 36.06 $cm^3/g$, respectively).

As illustrated in Figure 3 and Table 1, UiO-67-HCl has a 900 $m^2/g$ higher nitrogen gas accessible BET surface area than UiO-67-AA. The step in the isotherm of UiO-67-HCl around 0.15 a P/P° is due to defects.[50] For pristine UiO-67, the structure is expected to have a tetrahedral pore at 12 Å and an octahedral pore at 16 Å.[48, 60] As shown in the inset of Figure 3, UiO-67-AA contains two pores at 12.7 and 15.5 Å, consistent with Ui-67-AA. UiO-67-HCl contains the same pores as the AA counterpart, but also contains a considerable amount of larger pores (e.g., at 25 Å) due to defects.[50] Thus, UiO-67-AA and UiO-67-HCl are good isoreticular counterparts to UiO-66-AA and UiO-67-HCl.

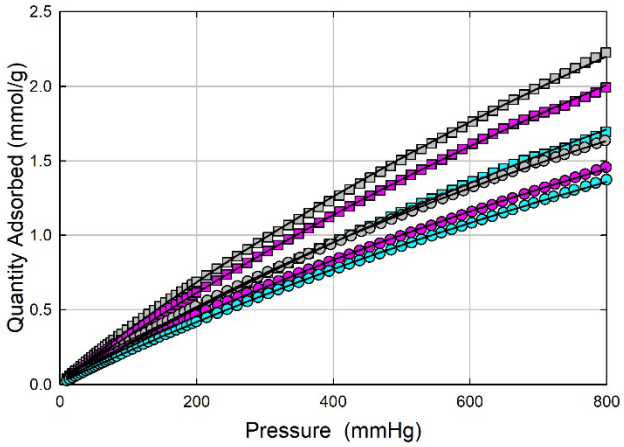


Figure 4: Carbon dioxide adsorption isotherms of UiO-67-AA (circles) and UiO-67-HCl (squares) at 278 K (grey) 283 K (pink) and 288 K (cyan). The fits from the Langmuir isotherm model are shown as black traces.

The carbon dioxide adsorption isotherms for UiO-67-AA and UiO-67-HCl (Figure 4 and Table 1) are more similar than different. The adsorption capacity ($Q_{max}$) differences is

due to the differences in their surface areas; there is a nearly linear relationship between the BET surface area and $Q_{max}$ for the four as-synthesized UiOs ($R^2$ = 0.96). Turning to the enthalpies of adsorption of carbon dioxide on these MOFs (Table 1, Table S1, and Table S2), UiO-67-HCl is 4.3 kJ/mol more exothermic than UiO-67-AA (–21.2 vs. –16.9 kJ/mol); this is contradictory to what was observed in UiO-66 (–20.9 vs. –24.9 kJ/mol).

Returning to our hypotheses for UiO-66, the data for UiO-67 indicates that pristine UiO-66 has a more favourable pore size and shape for confinement effects for carbon dioxide adsorption relative to UiO-67. If it was a structural effect due to a corner/edge, due to the pristine structure, then we would expect UiO-67-AA to outperform UiO-67-HCl. We propose that the smaller tetrahedral pore of UiO-66 is responsible for these effects. Interestingly, when the optimal pore size is not present, the defect-containing UiO-67-HCl outperforms the pristine UiO-67-HCl. This suggests that hydrogen bonding associated with the defects is beneficial.

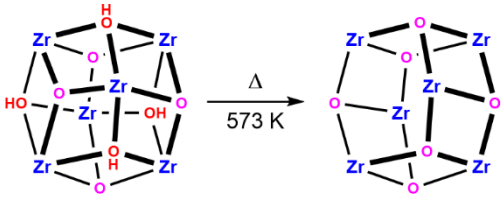


Figure 5: Dehydration of the zirconium node in UiO-based MOFs from $[Zr_6O_4(OH)_4]^{12+}$ to $[Zr_6O_6]^{12+}$ via the loss of two equivalence of water per node.

To better understand the pore-confinement effect and the role of defects, we dehydrated UiO-66 and UiO-67; in both MOFs, this converts the $Zr_6O_4(OH)_4^{12+}$ node to $Zr_6O_6^{12+}$ (Figure 5).[59] Dehydration creates open coordination sites on the node while also removing hydrogen bonding effects. These effects come from the acidic $\mu_3$-OH, or the terminal water/hydroxide molecules from defect sites; the latter hydroxide sites would likely undergo a dehydration reaction to form an oxo and water unit similar to the $\mu_3$-OH on the node (Figure 5). With that in mind, as-synthesized UiOs were heated at 573 K overnight (ΔUiOs; see SI for details). Neither the nitrogen gas accessible BET surface area (Table 1, Figure S3 & S4) nor the PSDs (Figure 6; Figure S7-S10 for PSD comparison) were considerably changed from the parent material.

The carbon dioxide enthalpies of adsorption (Table 1; see Figure S11 & S12 for isotherms) for the dehydrated UiO-66-AA and UiO-66-HCl are identical (–21 kJ/mol). Given the decrease in the enthalpy of adsorption for the former, this indicates that the hydroxylated node is a cooperative part of the confinement effect necessary to produce the high heats for UiO-66-AA; when the cooperative effect is not present (i.e., UiO-66-HCl vs. ΔUiO-66-HCl), the enthalpies are not affected by dehydration. These results suggests that when the hydrogen bonding is lost, then the confinement effect is not as strong or completely absent. We hypothesize that with the pristine pore structure and the presence of the $\mu_3$-OH, the electro negative oxygen of the carbon dioxide can interact with the acidic $\mu_3$-OH;[61] this works in concert with the tetrahedral pore shape/size to tightly bind carbon dioxide. The lack of any change in the adsorption enthalpies for UiO-66-HCl vs. ΔUiO-66-HCl is likely due to the dispersion interactions being similar in energy to the hydrogen bonding interactions; this can be seen in ΔUiO-67.

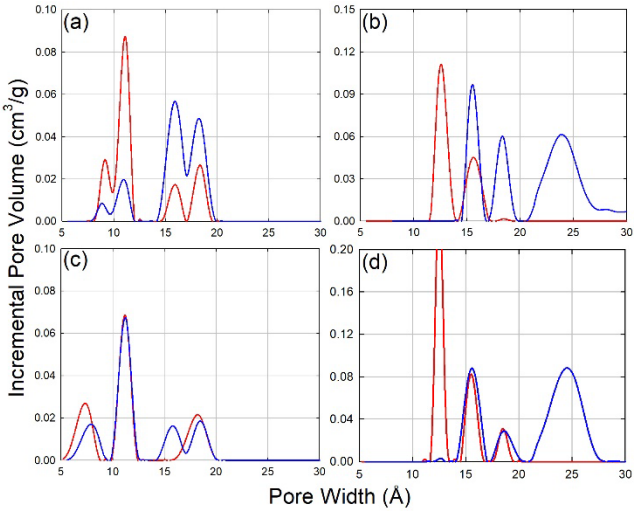


Figure 6: PSD of (a) ΔUiO-66-AA (red trace; the standard deviation of the fit is 4.66 $cm^3/g$), ΔUiO-66-HCl (blue trace; 1.19 $cm^3/g$); (b) ΔUiO-67-AA (red trace; 22.29 $cm^3/g$), ΔUiO-67-HCl (blue trace; 24.12 $cm^3/g$); (c) MeOH-UiO-66-AA (red trace; 6.11 $cm^3/g$), MeOH-UiO-66-HCl (blue trace; 5.35 $cm^3/g$); (d) MeOH-UiO-67-AA (red trace; 32.95 $cm^3/g$) MeOH-UiO-67-HCl (blue trace; 28.33 $cm^3/g$). See Figure S7-S10 for additional PSD comparisons.

When UiO-67 is dehydrated, then the enthalpies of adsorption also become identical (Table 1). However, both ΔUiO-67-AA and ΔUiO-67-HCl become notably less exothermic. Clearly, the presence of hydrogen bonding groups is important for higher enthalpies of adsorption.[61] The surprisingly small adsorption enthalpies suggest that the remaining dispersion interactions between carbon dioxide and the MOF are lower in ΔUiO-67 relative to ΔUiO-66. This is likely due to the electron withdrawing nature of Zr(IV). For UiO-66, the four Zr(IV) units coordinated to the BDC linker make the aryl ring electron deficient ($\delta^+$) thereby increasing the dispersion interactions to the oxygen atoms on carbon dioxide.[61] For UiO-67, two Zr(IV) acting on each aryl ring is insufficient to engender such strong effects. Thus, for UiO-67 hydrogen bonding is more beneficial for enhancing the carbon dioxide adsorption enthalpy, relative to UiO-66. This behaviour may be enhanced by the dehydration process that removes an electron donating oxygen atom from the node. This supports our hypothesis that hydrogen bonding is working in concert with the cooperative effects in UiO-66-AA.

In an attempt to exploit the hydrogen bonding and confinement effects, post synthetic modification was explored. Illustrated in Figure 7, Ameloot and co-workers demonstrated that soaking UiO-66 in methanol can produce two different types of defects.[56] In pristine UiO-66, linker solvolysis results in dissociation of one of the carboxylates on BDC from the node. This results in a terminal methanol/methoxy capping groups and an uncoordinated carboxylate/carboxylic acid. In defect-containing UiO-66, the terminal groups

are replaced with methanol/methoxy groups. To that end, the four as-synthesized and activated UiOs were soaked in methanol for 3 days (MeOH-UiOs).

The PSDs for MeOH-UiOs are shown in Figure 6c-d (Figure S5 & S6 contains the associated nitrogen gas adsorption isotherms). Relative to the parent MOF, MeOH-UiO-66-HCl shows the only significant difference in the PSDs (Figure 1, Figures S8) with the PSD looking more like UiO-66-AA (Figure S7 & S8) than UiO-66-HCl. In MeOH-UiO-66-HCl, 66% of the total pore volume is due to pores below 12 Å vs. 13% in UiO-66-HCl and 86% in UiO-66-AA. This suggests that the methanol/methoxy groups close off the pore between two nodes such that gas molecules behave as if the defects are repaired. This effect is not observed in the other three MOFs, which have PSDs similar to their parent material (Figures S7-S10). This also indicates that UiO-66-HCl is dominated by missing linker-based over node-based defects. If node-based defects dominated, then the PSD would be expected to remain relatively unchanged between UiO-66-HCl and MeOH-UiO-66-HCl.

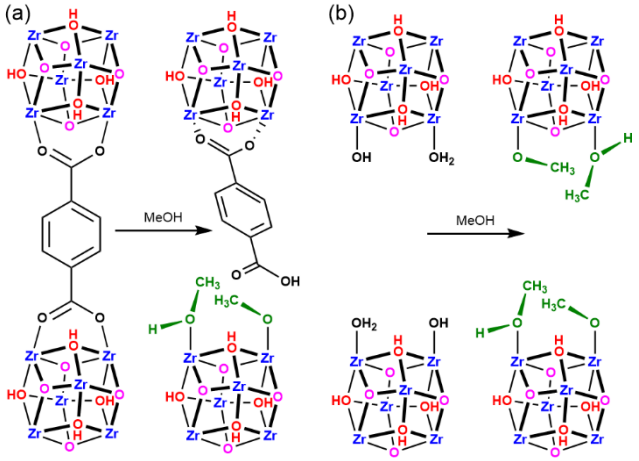


Figure 7: (a) Partial displacement of BDC via Methanol solvolysis in UiO-66-AA. (b) Substitution of defect terminal groups by methanol in UiO-66-HCl.[56]

Given the PSDs for the MeOH-UiOs (Figure 6), the biggest change in the extracted enthalpies of adsorption (Table 1; Figure S13 & S14) is observed for MeOH-UiO-66-HCl, which is nearly 8 kJ/mol (–20.9 vs. –28.4 kJ/mol) more exothermic than the parent MOF. We propose that this creates a confinement effect similar to that in UiO-66-AA, which is enhanced by the extra flexibility and hydrogen bonding capabilities of the methanol/methoxy groups. This can be further observed in the entropy of adsorption ($\Delta S_{ads}$; Table S2). MeOH-UiO-66-HCl has a $\Delta S_{ads}$ 18(4) J/molK lower (more ordered) than the other five UiO-66 samples. For the other three methanol-modified MOFs, either the solvolysis has a minor enhancement (MeOH-UiO-67-HCl), is an ineffective tool, or thermal activation reverses the solvolysis and thus no effect is observed (Figure S7-S10).

Although the dominating defect density in this work is missing linkers, missing nodes are possible. Van Der Voort has shown that UiO-66 can be synthesized with node-based defects as the dominant defects.[49] The enthalpies of adsorption were determined from isotherms at 273 and 298 K. The enthalpies ranged from 21 – 23 KJ/mol which indicates that missing linkers and methanol capping groups have a larger effect over missing nodes.

**4 Conclusions**

The work above demonstrates the structural features that are responsible for strong carbon dioxide adsorption in UiO-based MOFs. By extension, other MOFs that have similar structural features may also share these enhancements. Given this, we are currently investigating how further functionalizing defects in structurally similar MOFs can be used to improve the enthalpy of adsorption and adsorption selectivity. Additionally, we are exploring if the phenomena observed in this manuscript extends to gases beyond carbon dioxide.

## ASSOCIATED CONTENT

Synthesis of the UiOs, Powder X-ray diffractograms, Nitrogen gas adsorption isotherms (AIF files) and pore size distributions, carbon dioxide adsorption isotherms (AIF files), and isosteric heats of adsorption calculations are available in the supporting Information is available free of charge at XXXX.

## AUTHOR INFORMATION

### Corresponding Author

Michael J. Katz – Department of Chemistry, Memorial University of Newfoundland, St. John's, Newfoundland and Labrador, Canada A1B 3X7; orcid.org/0000-0002-7744-3956;
Email: mkatz@mun.ca

### Author Contributions

The manuscript was written through contributions of all authors. All authors have given approval to the final version of the manuscript. Supervision and funding acquisition (MJK), Investigation (MCL, AS), Visualization (all), Writing – original draft (MCL), editing (all).

## ABBREVIATIONS

AA-Acetic acid; BDC-terephthalate; BET-Brunauer, Emmett, Teller; BPDC-biphenyldicarboxylate; $K_{ads}$-gas adsorption equilibrium constant; MeOH-Methanol; MOF-Metal-organic framework; PSD-Pore size distribution; $Q_{ads}$-quantity adsorbed at pressure P; $Q_{max}$-maximum adsorption capacity; UiO-Universitetet i Oslo; Δ-thermally dehydrated; $\Delta H_{ads}$-Enthaply of adsorption, $\Delta S_{ads}$- Entropy of adsorption.

### Acknowledgement

The work was funded by the National Sciences and Engineering Research Council of Canada (NSERC) for funding through a Discovery Grant and Research Tools and Instruments Grant. The Research and Development Corporation of Newfoundland (RDC; now TCII) is acknowledged for providing a leverage grant. M.C.L would like to acknowledge Mitacs for funding through an Indigenous Research award and the Qalipu First Nations Student Support Program.

## REFERENCES

1. Houghton, J., *Global Warming: The Complete Briefing*. 5 ed.; Cambridge University Press: Cambridge, 2015.

2. Kolle, J. M.; Fayaz, M.; Sayari, A., Understanding the Effect of Water on $CO_2$ Adsorption. *Chem. Rev.* **2021,** *121* (13), 7280-7345.

3. Ebi, K. L.; Loladze, I., Elevated atmospheric $CO_2$ concentrations and climate change will affect our food's quality and quantity. *Lancet Planet Health* **2019,** *3* (7), e283-e284.

4. Abbass, K.; Qasim, M. Z.; Song, H.; Murshed, M.; Mahmood, H.; Younis, I., A review of the global climate change impacts, adaptation, and sustainable mitigation measures. *Environ. Sci. Pollut. Res.* **2022,** *29* (28), 42539-42559.

5. Davis, S. J.; Lewis, N. S.; Shaner, M.; Aggarwal, S.; Arent, D.; Azevedo, I. L.; Benson, S. M.; Bradley, T.; Brouwer, J.; Chiang, Y.-M., et al., Net-zero emissions energy systems. *Science* **2018,** *360* (6396), eaas9793.

6. Bataille, C. G. F., Physical and policy pathways to net-zero emissions industry. *WIREs Clim. Change* **2020,** *11* (2), e633.

7. Rogelj, J.; Geden, O.; Cowie, A.; Reisinger, A., Net-zero emissions targets are vague: three ways to fix. *Nature* **2021,** *591* (7850), 365-368.

8. Fankhauser, S.; Smith, S. M.; Allen, M.; Axelsson, K.; Hale, T.; Hepburn, C.; Kendall, J. M.; Khosla, R.; Lezaun, J.; Mitchell-Larson, E., et al., The meaning of net zero and how to get it right. *Nat. Clim. Change* **2022,** *12* (1), 15-21.

9. Gayen, D.; Chatterjee, R.; Roy, S., A review on environmental impacts of renewable energy for sustainable development. *Int. J. Environ. Sci. Technol.* **2024,** *21* (5), 5285-5310.

10. Sai Bhargava Reddy, M.; Ponnamma, D.; Sadasivuni, K. K.; Kumar, B.; Abdullah, A. M., Carbon dioxide adsorption based on porous materials. *RSC Advances* **2021,** *11* (21), 12658-12681.

11. Terlouw, T.; Bauer, C.; Rosa, L.; Mazzotti, M., Life cycle assessment of carbon dioxide removal technologies: a critical review. *Energy Environ. Sci.* **2021,** *14* (4), 1701-1721.

12. Hu, Z.; Wang, Y.; Shah, B. B.; Zhao, D., $CO_2$ Capture in Metal–Organic Framework Adsorbents: An Engineering Perspective. *Adv. Sustainable Syst.* **2019,** *3* (1), 1800080.

13. Sumida, K.; Rogow, D. L.; Mason, J. A.; McDonald, T. M.; Bloch, E. D.; Herm, Z. R.; Bae, T.-H.; Long, J. R., Carbon Dioxide Capture in Metal–Organic Frameworks. *Chem. Rev.* **2012,** *112* (2), 724-781.

14. Garba, M. D.; Usman, M.; Khan, S.; Shehzad, F.; Galadima, A.; Ehsan, M. F.; Ghanem, A. S.; Humayun, M., $CO_2$ towards fuels: A review of catalytic conversion of carbon dioxide to hydrocarbons. *J. Environ. Chem. Eng.* **2021,** *9* (2), 104756.

15. Siegelman, R. L.; Kim, E. J.; Long, J. R., Porous materials for carbon dioxide separations. *Nat. Mater.* **2021,** *20* (8), 1060-1072.

16. Bose, S.; Sengupta, D.; Rayder, T. M.; Wang, X.; Kirlikovali, K. O.; Sekizkardes, A. K.; Islamoglu, T.; Farha, O. K., Challenges and Opportunities: Metal–Organic Frameworks for Direct Air Capture. *Adv. Funct. Mater.* **2023**, 2307478.

17. Sanz-Pérez, E. S.; Murdock, C. R.; Didas, S. A.; Jones, C. W., Direct Capture of $CO_2$ from Ambient Air. *Chem. Rev.* **2016,** *116* (19), 11840-11876.

18. Li, Z.; Liu, P.; Ou, C.; Dong, X., Porous Metal–Organic Frameworks for Carbon Dioxide Adsorption and Separation at Low Pressure. *ACS Sustainable Chem. Eng.* **2020,** *8* (41), 15378-15404.

19. Chowdhury, S.; Kumar, Y.; Shrivastava, S.; Patel, S. K.; Sangwai, J. S., A Review on the Recent Scientific and Commercial Progress on the Direct Air Capture Technology to Manage Atmospheric $CO_2$ Concentrations and Future Perspectives. *Energy Fuels* **2023,** *37* (15), 10733-10757.

20. Lawrence, M. C.; Katz, M. J., Analysis of the Water Adsorption Isotherms in UiO-Based Metal–Organic Frameworks. *J. Phys. Chem. C* **2022,** *126* (2), 1107-1114.

21. Lin, J.-B.; Nguyen, T. T. T.; Vaidhyanathan, R.; Burner, J.; Taylor, J. M.; Durekova, H.; Akhtar, F.; Mah, R. K.; Ghaffari-Nik, O.; Marx, S., et al., A scalable metal-organic framework as a durable physisorbent for carbon dioxide capture. *Science* **2021,** *374* (6574), 1464-1469.

22. Rajendran, A.; Shimizu, G. K. H.; Woo, T. K., The Challenge of Water Competition in Physical Adsorption of $CO_2$ by Porous Solids for Carbon Capture Applications – A Short Perspective. *Adv. Mater.* **2024,** *36* (12), 2301730.

23. Bell, J. G.; Benham, M. J.; Thomas, K. M., Adsorption of Carbon Dioxide, Water Vapor, Nitrogen, and Sulfur Dioxide on Activated Carbon for Capture from Flue Gases: Competitive Adsorption and Selectivity Aspects. *Energy Fuels* **2021,** *35* (9), 8102-8116.

24. Samanta, A.; Zhao, A.; Shimizu, G. K. H.; Sarkar, P.; Gupta, R., Post-Combustion CO2 Capture Using Solid Sorbents: A Review. *Ind. Eng. Chem. Res.* **2012,** *51* (4), 1438-1463.

25. Li, J.-R.; Ma, Y.; McCarthy, M. C.; Sculley, J.; Yu, J.; Jeong, H.-K.; Balbuena, P. B.; Zhou, H.-C., Carbon dioxide capture-related gas adsorption and separation in metal-organic frameworks. *Coord. Chem. Rev.* **2011,** *255* (15), 1791-1823.

26. Sabouni, R.; Kazemian, H.; Rohani, S., Carbon dioxide capturing technologies: a review focusing on metal organic framework materials (MOFs). *Environ. Sci. Pollut. Res.* **2014,** *21* (8), 5427-5449.

27. Ifraemov, R.; Mukhopadhyay, S.; Hod, I., Photo-Assisted Electrochemical $CO_2$ Reduction to $CH_4$ Using a Co-Porphyrin-Based Metal–Organic Framework. *Solar RRL* **2023,** *7* (5), 2201068.

28. Ding, M.; W. Flaig, R.; Jiang, H.-L.; M. Yaghi, O., Carbon capture and conversion using metal–organic frameworks and MOF-based materials. *Chem. Soc. Rev.* **2019,** *48* (10), 2783-2828.

29. Shimoni, R.; Shi, Z.; Binyamin, S.; Yang, Y.; Liberman, I.; Ifraemov, R.; Mukhopadhyay, S.; Zhang, L.; Hod, I., Electrostatic Secondary-Sphere Interactions That Facilitate Rapid and Selective Electrocatalytic $CO_2$ Reduction in a Fe-Porphyrin-Based Metal–Organic Framework. *Angew. Chem. Int. Ed.* **2022,** *61* (32), e202206085.

30. Hughes, R.; Kotamreddy, G.; Bhattacharyya, D.; Parker, S. T.; Dods, M. N.; Long, J. R.; Omell, B.; Matuszewski, M., Development of a chemistry-based isotherm model and techno-economic optimization of a moving bed process for $CO_2$ capture using a functionalized metal-organic framework. *Chem. Eng. Sci.* **2024,** *287*, 119679.

31. Nguyen, T. T. T.; Shimizu, G. K. H.; Rajendran, A., CO2/N2 separation by vacuum swing adsorption using a metal–organic framework, CALF-20: Multi-objective optimization and experimental validation. *Chem. Eng. J.* **2023,** *452*, 139550.

32. Luo, J.-P.; Zhang, J.; Yin, N.; Wang, T.-P.; Tan, Z.-C.; Han, W.; Shi, Q., An experimental strategy for evaluating the energy performance of metal–organic framework-based carbon dioxide adsorbents. *Chem. Eng. J.* **2022,** *442*, 136210.

33. Mahajan, S.; Lahtinen, M., Recent progress in metal-organic frameworks (MOFs) for CO2 capture at different pressures. *J. Environ. Chem. Eng.* **2022,** *10* (6), 108930.

34. Mason, J. A.; Sumida, K.; Herm, Z. R.; Krishna, R.; Long, J. R., Evaluating metal–organic frameworks for post-combustion carbon dioxide capture via temperature swing adsorption. *Energy Environ. Sci.* **2011,** *4* (8), 3030-3040.

35. Hedin, N.; Andersson, L.; Bergström, L.; Yan, J., Adsorbents for the post-combustion capture of $CO_2$ using rapid temperature swing or vacuum swing adsorption. *Appl. Energy* **2013,** *104*, 418-433.

36. Zhao, R.; Liu, L.; Zhao, L.; Deng, S.; Li, S.; Zhang, Y., A comprehensive performance evaluation of temperature swing adsorption for post-combustion carbon dioxide capture. *Renewable and Sustainable Energy Reviews* **2019,** *114*, 109285.

37. Burns, T. D.; Pai, K. N.; Subraveti, S. G.; Collins, S. P.; Krykunov, M.; Rajendran, A.; Woo, T. K., Prediction of MOF Performance in Vacuum Swing Adsorption Systems for Postcombustion $CO_2$ Capture Based on Integrated Molecular Simulations, Process Optimizations, and Machine Learning Models. *Environ. Sci. Technol.* **2020,** *54* (7), 4536-4544.

38. Chen, Z.; Kirlikovali, K. O.; Shi, L.; Farha, O. K., Rational design of stable functional metal–organic frameworks. *Mater. Horiz.* **2023,** *10* (9), 3257-3268.

39. Lee, S. J.; Telfer, S. G., Multicomponent Metal-Organic Frameworks. *Angew. Chem. Int. Ed.* **2023,** *62* (44), e202306341.

40. Zhu, Z.; Tsai, H.; Parker, S. T.; Lee, J.-H.; Yabuuchi, Y.; Jiang, H. Z. H.; Wang, Y.; Xiong, S.; Forse, A. C.; Dinakar, B., et al., High-Capacity, Cooperative $CO_2$ Capture in a Diamine-Appended Metal–Organic Framework through a Combined Chemisorptive and Physisorptive Mechanism. *J. Am. Chem. Soc.* **2024,** *146* (9), 6072-6083.

41. Mohan, B.; Virender; Kadiyan, R.; Kumar, S.; Gupta, V.; Parshad, B.; Solovev, A. A.; Pombeiro, A. J. L.; Kumar, K.; Sharma, P. K., Carbon dioxide capturing activities of porous metal-organic frameworks (MOFs). *Microporous Mesoporous Mater.* **2024,** *366*, 112932.

42. Ho, C.-H.; Paesani, F., Elucidating the Competitive Adsorption of $H_2O$ and $CO_2$ in CALF-20: New Insights for Enhanced Carbon Capture

Metal–Organic Frameworks. *ACS Appl. Mater. Interfaces* **2023,** *15* (41), 48287-48295.

43. Kataria, B.; Jeyaseelan, C., Chapter 10 - Metal Organic Frameworks as an Efficient Method for Carbon dioxide capture. In *Green Sustainable Process for Chemical and Environmental Engineering and Science*, Inamuddin, D.; Altalhi, T., Eds. Elsevier: 2023; pp 211-230.

44. Liang, Z.; Ou, Y.; El-Sayed, E.-S. M.; Su, K.; Wang, W.; Yuan, D., Effect of Functional Groups on Low-Concentration Carbon Dioxide Capture in UiO-66-Type Metal–Organic Frameworks. *Inorg. Chem.* **2023,** *62* (21), 8309-8314.

45. Biswas, S.; Van Der Voort, P., A General Strategy for the Synthesis of Functionalised UiO-66 Frameworks: Characterisation, Stability and $CO_2$ Adsorption Properties. *Eur. J. Inorg. Chem.* **2013,** *2013* (12), 2154-2160.

46. Cavka, J. H.; Jakobsen, S.; Olsbye, U.; Guillou, N.; Lamberti, C.; Bordiga, S.; Lillerud, K. P., A New Zirconium Inorganic Building Brick Forming Metal Organic Frameworks with Exceptional Stability. *J. Am. Chem. Soc.* **2008,** *130* (42), 13850-13851.

47. Tatay, S.; Martínez-Giménez, S.; Rubio-Gaspar, A.; Gómez-Oliveira, E.; Castells-Gil, J.; Dong, Z.; Mayoral, Á.; Almora-Barrios, N.; M. Padial, N.; Martí-Gastaldo, C., Synthetic control of correlated disorder in UiO-66 frameworks. *Nat. Commun.* **2023,** *14* (1), 6962.

48. Winarta, J.; Shan, B.; McIntyre, S. M.; Ye, L.; Wang, C.; Liu, J.; Mu, B., A Decade of UiO-66 Research: A Historic Review of Dynamic Structure, Synthesis Mechanisms, and Characterization Techniques of an Archetypal Metal–Organic Framework. *Cryst. Growth Des.* **2020,** *20* (2), 1347-1362.

49. Feng, X.; Jena, H. S.; Krishnaraj, C.; Arenas-Esteban, D.; Leus, K.; Wang, G.; Sun, J.; Rüscher, M.; Timoshenko, J.; Roldan Cuenya, B., et al., Creation of Exclusive Artificial Cluster Defects by Selective Metal Removal in the (Zn, Zr) Mixed-Metal UiO-66. *J. Am. Chem. Soc.* **2021,** *143* (51), 21511-21518.

50. Katz, M.; Brown, Z.; Colón, Y.; Siu, P.; Scheidt, K.; Snurr, R.; Hupp, J.; Farha, O., A facile synthesis of UiO-66, UiO-67 and their derivatives. *Chem. Commun.* **2013,** *49*, 9449-9451.

51. Sannes, D. K.; Øien-Ødegaard, S.; Aunan, E.; Nova, A.; Olsbye, U., Quantification of Linker Defects in UiO-Type Metal–Organic Frameworks. *Chem. Mater.* **2023,** *35* (10), 3793-3800.

52. Tan, K.; Pandey, H.; Wang, H.; Velasco, E.; Wang, K.-Y.; Zhou, H.-C.; Li, J.; Thonhauser, T., Defect Termination in the UiO-66 Family of Metal–Organic Frameworks: The Role of Water and Modulator. *J. Am. Chem. Soc.* **2021,** *143* (17), 6328-6332.

53. Wang, Y.; Peng, C.; Jiang, T.; Li, X., Research progress of defect-engineered UiO-66(Zr) MOFs for photocatalytic hydrogen production. *Front. Energy* **2021,** *15* (3), 656-666.

54. Schaate, A.; Roy, P.; Godt, A.; Lippke, J.; Waltz, F.; Wiebcke, M.; Behrens, P., Modulated Synthesis of Zr-Based Metal–Organic Frameworks: From Nano to Single Crystals. *Chem. Eur. J.* **2011,** *17* (24), 6643-6651.

55. Valenzano, L.; Civalleri, B.; Chavan, S.; Bordiga, S.; Nilsen, M. H.; Jakobsen, S.; Lillerud, K. P.; Lamberti, C., Disclosing the Complex Structure of UiO-66 Metal Organic Framework: A Synergic Combination of Experiment and Theory. *Chem. Mater.* **2011,** *23* (7), 1700-1718.

56. Marreiros, J.; Caratelli, C.; Hajek, J.; Krajnc, A.; Fleury, G.; Bueken, B.; De Vos, D. E.; Mali, G.; Roeffaers, M. B. J.; Van Speybroeck, V., et al., Active Role of Methanol in Post-Synthetic Linker Exchange in the Metal–Organic Framework UiO-66. *Chem. Mater.* **2019,** *31* (4), 1359-1369.

57. Audu, C. O.; Nguyen, H. G. T.; Chang, C.-Y.; Katz, M. J.; Mao, L.; Farha, O. K.; Hupp, J. T.; Nguyen, S. T., The dual capture of $As^{V}$ and $As^{III}$ by UiO-66 and analogues. *Chem. Sci.* **2016,** *7* (10), 6492-6498.

58. Liang, W.; Coghlan, C. J.; Ragon, F.; Rubio-Martinez, M.; D'Alessandro, D. M.; Babarao, R., Defect engineering of UiO-66 for $CO_2$ and $H_2O$ uptake – a combined experimental and simulation study. *Dalton Trans.* **2016,** *45* (11), 4496-4500.

59. Shearer, G. C.; Chavan, S.; Bordiga, S.; Svelle, S.; Olsbye, U.; Lillerud, K. P., Defect Engineering: Tuning the Porosity and Composition of the Metal–Organic Framework UiO-66 via Modulated Synthesis. *Chem. Mater.* **2016,** *28* (11), 3749-3761.

60. Zhao, W.; Zhang, C.; Yan, Z.; Zhou, Y.; Li, J.; Xie, Y.; Bai, L.; Jiang, L.; Li, F., Preparation, characterization, and performance evaluation of UiO-66 analogues as stationary phase in HPLC for the separation of substituted benzenes and polycyclic aromatic hydrocarbons. *PLoS One* **2017,** *12* (6), e0178513.

61. Grissom, T. G.; Driscoll, D. M.; Troya, D.; Sapienza, N. S.; Usov, P. M.; Morris, A. J.; Morris, J. R., Molecular-Level Insight into $CO_2$ Adsorption on the Zirconium-Based Metal–Organic Framework, UiO-66: A Combined Spectroscopic and Computational Approach. *J. Phys. Chem. C* **2019,** *123* (22), 13731-13738.

**TOC graphic:**